

# Halogen Bonding versus Hydrogen Bonding in Driving Self-Assembly and Performance of Light-Responsive Supramolecular Polymers

Arri Priimagi,\* Gabriella Cavallo, Alessandra Forni, Mikael Gorynsztejn–Leben, Matti Kaivola, Pierangelo Metrangolo,\* Roberto Milani, Atsushi Shishido, Tullio Pilati, Giuseppe Resnati,\* and Giancarlo Terraneo

Halogen bonding is arguably the least exploited among the many non-covalent interactions used in dictating molecular self-assembly. However, its directionality renders it unique compared to ubiquitous hydrogen bonding. Here, the role of this directionality in controlling the performance of light-responsive supramolecular polymers is highlighted. In particular, it is shown that light-induced surface patterning, a unique phenomenon occurring in azobenzene-containing polymers, is more efficient in halogen-bonded polymer–azobenzene complexes than in the analogous hydrogen-bonded complexes. A systematic study is performed on a series of azo dyes containing different halogen or hydrogen bonding donor moieties, complexed to poly(4-vinylpyridine) backbone. Through single-atom substitution of the bond-donor, control of both the strength and the nature of the noncovalent interaction between the azobenzene units and the polymer backbone is achieved. Importantly, such substitution does not significantly alter the electronic properties of the azobenzene units, hence providing us with unique tools in studying the structure–performance relationships in the light-induced surface deformation process. The results represent the first demonstration of light-responsive halogen-bonded polymer systems and also highlight the remarkable potential of halogen bonding in fundamental studies of photoresponsive azobenzene-containing polymers.

## 1. Introduction

Light-induced surface patterning is a unique feature of azobenzene-containing materials, in which the photoisomerization of the azobenzene chromophores initiates mass transport over micrometer distances.<sup>[1,2]</sup> This simple, all-optical, and reversible process requires only a single fabrication step to inscribe high-quality surface relief gratings (SRGs), showing potential for numerous applications in photonics and nanotechnology.<sup>[2–6]</sup> The grating formation has been studied in various azobenzene-containing systems,<sup>[7–9]</sup> and in the past few years, supramolecular functionalization strategies have emerged as facile tools to design photoresponsive polymers that undergo efficient light-induced mass transport.<sup>[10–12]</sup> Furthermore, the inherent tunability of supramolecular chemistry provides unprecedented possibilities for fundamental studies of light-induced mass transport in photoresponsive polymers, the fundamental mechanism and

Dr. A. Priimagi, M. Gorynsztejn–Leben, Prof. M. Kaivola  
Department of Applied Physics  
Aalto University  
P.O. Box 13500, FI-00076 Aalto, Finland  
E-mail: arri.priimagi@aalto.fi  
Dr. A. Priimagi, Prof. A. Shishido  
Chemical Resources Laboratory  
Tokyo Institute of Technology  
R1-12 Nagatsuta, Midori-ku, Yokohama 226-8503, Japan  
Dr. G. Cavallo, Prof. P. Metrangolo, Dr. T. Pilati, Prof. G. Resnati,  
Dr. G. Terraneo  
NFM Lab, DCMIC “Giulio Natta”  
Politecnico di Milano  
Via Mancinelli 7, I-20131 Milano, Italy  
E-mail: pierangelo.metrangolo@polimi.it; giuseppe.resnati@polimi.it

Dr. A. Forni, Dr. T. Pilati, Prof. G. Resnati  
ISTM-CNR  
Università degli Studi di Milano  
Via Golgi 19, I-20133 Milano, Italy  
Prof. P. Metrangolo, Dr. R. Milani, Prof. G. Resnati,  
Dr. G. Terraneo  
Center for Nano Science and Technology@Polimi  
Istituto Italiano di Tecnologia  
via Pascoli 70/3, I-20133 Milano, Italy  
Prof. P. Metrangolo, Dr. R. Milani  
VTT, Technical Research Centre of Finland  
Tietotie 2, FIN-02044 VTT, Finland



DOI: 10.1002/adfm.201200135

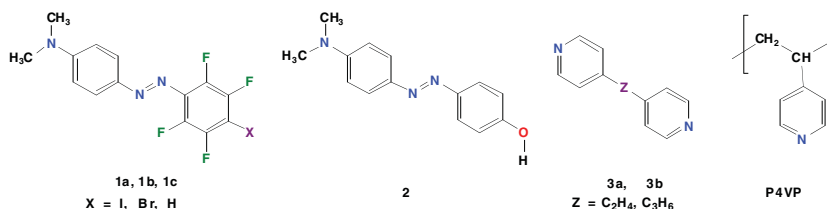
structure–function relationships of which remain unsettled up to date.<sup>[13,14]</sup> Herein, we show that halogen bonding is a viable tool in designing high-performance supramolecular polymers for light-induced surface patterning. In fact, halogen bonding, because of its directionality and tuneable interaction strength, provides unique possibilities for fundamental studies of photoresponsive polymers, and halogen-bonded supramolecular polymers compare favourably and may even outperform analogous hydrogen-bonded systems in the SRG formation efficiency.

Halogen bonding<sup>[15]</sup> occurs between the positive region of the electrostatic potential surface of halogen atoms, which function as electrophilic species, and neutral or anionic Lewis bases.<sup>[16]</sup> Among the many noncovalent interactions that are commonly used to direct the formation of supramolecular assemblies, halogen bonding is arguably the least exploited, which is surprising given its potentially powerful analogy to ubiquitous hydrogen bonding.<sup>[17]</sup> In spite of this, halogen bonding has been convincingly used to control the self-assembly of diverse host-guest solids, with applications ranging from liquid-crystalline,<sup>[18–21]</sup> porous,<sup>[22,23]</sup> magnetic,<sup>[24]</sup> and organic phosphorescent materials,<sup>[25]</sup> to ion pair recognition,<sup>[26]</sup> biomolecular engineering,<sup>[27]</sup> and chemical separation.<sup>[28]</sup> In particular, halogen bonding is nowadays considered among the most valued tools in the field of crystal engineering because of its high strength, specificity, and directionality, which has allowed designing very complex structures with a high degree of accuracy and precision.<sup>[29]</sup>

Examples of halogen bonding involving polymeric donors and/or acceptors are extremely rare. In 2002 we reported the self-assembly of poly(4-vinylpyridine) with various  $\alpha,\omega$ -diodoperfluoroalkanes into fluorous supramolecular polymers.<sup>[30]</sup> Later on, applications of polymeric halogen-bonded materials have appeared in the fields of molecularly imprinted polymers,<sup>[31]</sup> topochemical polymerization,<sup>[32]</sup> and layer-by-layer assembly.<sup>[33]</sup>

Given that hydrogen bonding has been widely and successfully exploited in the design of functional and stimuli-responsive polymeric materials,<sup>[34–38]</sup> it appears reasonable to predict that halogen bonding holds a great potential for the design of a new class of analogous systems. Importantly, these two noncovalent interactions also display significant differences. Firstly, halogen bonding is more directional than hydrogen bonding<sup>[39]</sup> and has already proven effective in the design and synthesis of topologically complex structures.<sup>[40]</sup> Secondly, its interaction strength can be fine tuned by properly choosing the halogen atom that takes part in the bond formation without significantly changing the electronic structure of the compound.<sup>[41]</sup>

In the present work, the above-mentioned features of halogen bonding are shown to provide unique possibilities in understanding and controlling the properties of stimuli-responsive supramolecular polymers for light-induced surface patterning. We have designed halogen-bonded supramolecular polymers, which, by proper single atom mutation in the halogen bonding-donor moiety, allowed us to probe the role of both the nature and the strength of the noncovalent bonding on the SRG formation efficiency. We also compared the halogen-bonded systems



**Scheme 1.** Chemical structures of the azobenzene derivatives **1a–c** and **2** and the bis-pyridine compounds 1,2-di(4-pyridyl)ethane (**3a**) and 1,3-di(4-pyridyl)propane (**3b**) selected as model compounds for the polymer P4VP.

to previously established phenol–pyridine hydrogen-bonded systems, and showed that as a likely consequence of the higher directionality of halogen bonding, halogen-bonded complexes exhibit higher patterning efficiency than the hydrogen-bonded systems. The study is complemented by theoretical calculations and crystallographic investigations, which further enlighten the different performances displayed by halogen- and hydrogen-bonded systems.

## 2. Results

### 2.1. Systems Design

The similarities of hydrogen bonding and halogen bonding allowed us to use the same polymer host, poly(4-vinyl pyridine) (P4VP;  $M_w \approx 1000 \text{ g mol}^{-1}$ ), as a bond acceptor matrix for both interactions. It has already been demonstrated that P4VP efficiently self-assembles with hydrogen and halogen bond-donor molecules.<sup>[30,38]</sup> In the chromophore design, we made use of the unique possibility provided by halogen bonding to fine tune the nature and strength of the polymer–dye interaction by single halogen atom mutation on the tetrafluorobenzene ring. We synthesized the azobenzene derivatives **1a–c** shown in **Scheme 1**. The derivatives **1a** and **1b** are expected to form medium-to-weak halogen bonds with P4VP,<sup>[30,41]</sup> while **1c** is expected to form a medium-to-weak hydrogen bond with P4VP because of the acidic hydrogen atom of the tetrafluorobenzene ring. Hence the compound **1c** functions as a control molecule unable to form halogen bonds. Moreover, in order to compare the performance of halogen bonding and hydrogen bonding in SRG formation, the commercially available azobenzene derivative **2** was also chosen as a reference. Despite its somewhat different chemical structure with respect to **1a–c**, the phenol-containing **2** serves as an excellent reference since supramolecular polymers based on the phenol/pyridine supramolecular synthon have already proven to be efficient for photoinduced SRG formation,<sup>[42–45]</sup> and since its binding strength to P4VP is still higher than that shown by the halogenated dyes (cf. below), even when lacking fluorination of the benzene ring.

### 2.2. Theoretical Modelling

In order to validate our design assumptions and verify the occurrence, nature, and strength of the involved noncovalent

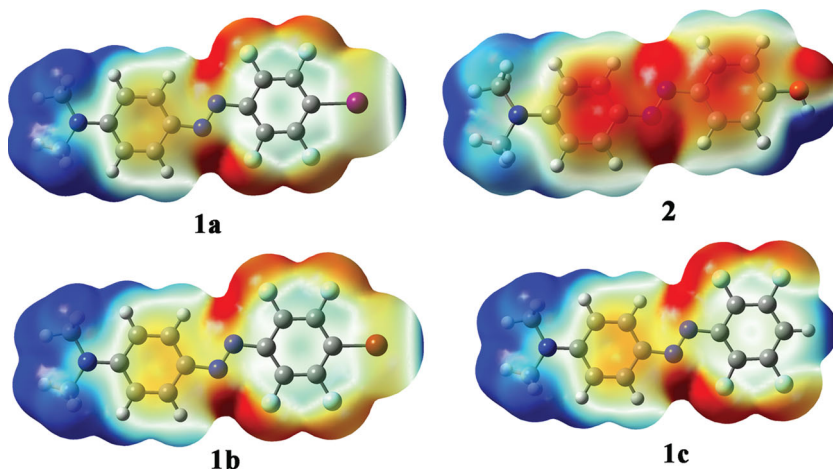


**Figure 1.** Plots of the electrostatic potential of the compounds **1a–c** and **2**. Potentials are mapped on the respective isosurfaces (0.001 a.u.) of electron density. Values of electrostatic potential range from  $-0.03$  (red) to  $0.03$  (blue) a.u. Atom color scheme: C, gray; H, light gray; N, dark blue; O, red; F, sky blue, I, magenta.

bonds, we modelled the P4VP–azobenzene systems using density functional theory (DFT). We calculated the interaction energies between the dyes in Scheme 1 and 4-methylpyridine, which functions as a model compound for the polymeric electron donor. The interaction strengths were computed as the difference between the energy of the bonded dimers and the sum of the energies of the single monomers. The energies calculated for the dimers of the iodine- and bromine-containing azo-dyes **1a** and **1b** ( $\Delta E_{\text{BSE}} = -5.135$  and  $-3.501$  kcal mol $^{-1}$ , respectively) are perfectly in line with those calculated for some analogous pyridine–halotetrafluorobenzene complexes.<sup>[20,46]</sup> Similarly, the interaction energies between 4-methylpyridine and the dyes **1c** and **2** ( $\Delta E_{\text{BSE}} = -3.930$  and  $-10.053$  kcal mol $^{-1}$ , respectively) correspond to values typical of medium-to-strong hydrogen bonds.<sup>[47]</sup>

The calculated interaction energies imply that the hydrogen-bonded dimer of **2** with 4-methylpyridine is more stable than the analogous halogen-bonded dimer formed with **1a**. However, as brought out by Politzer,<sup>[39]</sup> halogen bonding is more directional than hydrogen bonding. The reason for this is illustrated in **Figure 1**: Both the iodine and hydrogen atoms of the dyes **1a** and **2** display positively charged outer regions, which explains their capability to interact with negatively charged sites. But while the dark blue positively charged region is narrowly localized along the extension of the C–I bond of the iodine atom of **1a**, it is hemispherically distributed around the phenolic hydrogen atom of **2** and even spread over the nearby hydrogen atom in the *ortho* position of the phenol ring. Similarly, a narrower positively charged region is found on the bromine atom of **1b** compared to the hydrogen atom in the *para* position of the tetrafluorobenzene ring of **1c**, although both dyes were found to have similar interaction energies with 4-methylpyridine. This is highly pertinent because halogen bonding has been reported to successfully compete with hydrogen bonding in building up supramolecular architectures, even in spite of its lower or comparable interaction strength.<sup>[48]</sup>

The photoinduced surface patterning is driven by *trans–cis–trans* photoisomerization cycling of the azobenzene moieties, which in turn is affected by their dipole moments and spectroscopic properties.<sup>[49]</sup> The UV-vis absorption spectra of the dyes **1a–c** in dilute dimethylformamide (DMF) solutions are very similar (see Supporting Information, Figure S2), and significantly red-shifted when compared to the spectrum of **2**. This suggests that due to the strong electron-withdrawing character of the fluorinated aromatic ring, the dyes **1a–c** all have similar dipole moments, which are higher than that of **2**. This is supported by DFT calculations, according to which the dipole moments are 7.3, 7.5, 6.4, and 3.8 D in vacuum, and 10.2, 10.5, 8.9, and 5.7 D in DMF solution for **1a**, **1b**, **1c**, and **2**, respectively. The absorption spectra were then computed by time-dependent DFT, which reproduced the experimentally observed trend with the maximum absorption wavelength decreasing in the order **1a**  $\approx$  **1b**  $>$  **1c**  $\gg$  **2** (see Supporting Information, Table S1). We note that the similar electronic structure of the dyes **1a–c** is central for the present study, allowing us to distinguish the roles of nature and strength of the polymer–dye interaction from other factors affecting the photoinduced surface patterning.

### 2.3. Single Crystal X-ray Diffraction Studies

To have a model of the P4VP–azobenzene systems, we co-crystallized **1a–c** and **2** with the bis-pyridine derivatives shown in Scheme 1. Good-quality single crystals of the halogen-bonded complex **4** were obtained upon evaporation of a 2:1 chloroform solution of **1a** and **3a**. The differential scanning calorimetry (DSC) study of those crystals revealed a unique sharp melting endotherm at 465 K, which is higher than those of the starting materials (**1a**: 456 K; **3a**: 383 K), thus confirming the formation of a new chemical species rather than a mechanical mixture of the two starting compounds. The single crystal X-ray analysis of **4** revealed details of the supramolecular organization of the two components in the crystal lattice (**Figure 2**, top).

The components are held together in trimers by halogen bonds between the two nitrogen atoms of **3a** and the iodine atoms of two distinct **1a** molecules, explaining the observed 1:2 ratio. The N $\cdots$ I distances are 2.807(2) Å and 2.818(2) Å, corresponding to ca. 20% contraction with respect to the sum of the van der Waals radii for N and I.<sup>[50]</sup> The two C–I $\cdots$ N angles are 173.47(7) $^{\circ}$  and 170.45(7) $^{\circ}$ , which are perfectly consistent with the expected directionality of halogen bonds.<sup>[51]</sup>

The hydrogen-bonded complex **5** between **2** and **3b** was isolated as pale orange crystals with a melting point at 446 K, in between those of the starting compounds (**2**: 479 K; **3b**: 336 K). The supramolecular structure of **5** is sustained by the N $\cdots$ H–O interaction where **3b** functions as a bidentate hydrogen bond acceptor bridging two different molecules of **2**. The N $\cdots$ O and N $\cdots$ H distances are 2.703(2) Å and 1.73(3) Å, respectively,

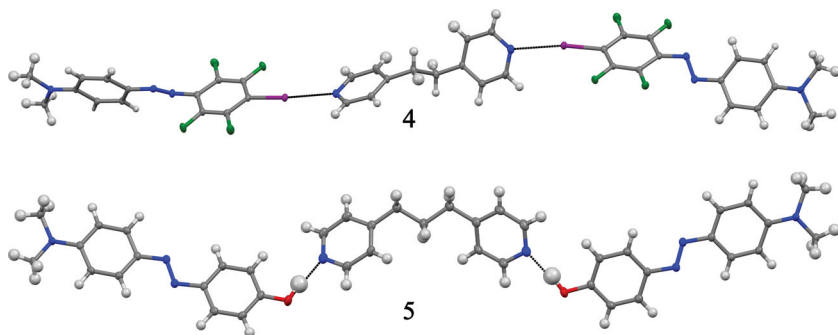


**Figure 2.** Halogen and hydrogen bonding drive the self-assembly of the azobenzenes **1a** and **2** and the bis-pyridine derivatives 1,2-di(4-pyridyl)ethane (**3a**) and 1,3-di(4-pyridyl)propane (**3b**) into the trimeric supramolecular structures **4** and **5**, respectively. Colors are as follows: C, gray; H, light gray; N, sky blue; O, red; F, green; I, magenta.

with an O–H···N angle of 168(2)° (Figure 2, bottom) and a C–O···N angle of 117.70(9)°.

Based on the solid-state structures of the two model systems **4** and **5** described above, it is evident that the geometries of the halogen-bonded and hydrogen-bonded complexes are quite different. The bis-pyridine molecule is almost collinear with the halogen-bonded iodotetrafluorobenzene of **1a**, as a consequence of the fact that halogen bonding essentially occurs along the extension of the C–I bond, i.e., the angle C–I···N is usually close to 180° (see Supporting Information, Figure S9). Instead, no such alignment is observed in the corresponding hydrogen-bonded system (the angle C–O···N is usually close to 120°, see Supporting Information, Figure S10).

We did not obtain good quality single crystals for the complex between **1a** and **3b**. However, from a 2:1 acetone solution of the starting components, we obtained the microcrystalline powder **6**, melting at 445 K. Also in this case, the melting temperature is different from those of the two starting compounds (**1a**: 456 K; **3b**: 336 K), which again proves that **6** is not a simple mechanical mixture of **1a** and **3b**. Moreover, the <sup>1</sup>H-NMR analysis in chloroform solution confirmed the expected 2:1 ratio between the starting compounds in the complex **6**.

The dyes **1b** and **1c** did not afford azobenzene–bipyridine complexes under the same co-crystallization procedures, instead, **1b** crystallized as a pure compound. This is consistent with theoretical modelling that **1b** and **1c** are less effective than **1a** in establishing non-covalent bonds with pyridyl moieties. A further indication of this came from the solid-state ball milling syntheses of complexes involving the azobenzene derivatives **1a–c**, **2** and the bis-pyridine **3b**: Melting point analysis revealed that the complexes **5** and **6** were formed after ball milling the starting compounds for 60 min at 30 Hz, whereas simple mechanical binary mixtures were obtained when the compounds **1b** and **1c** were used.

The noncovalent interactions between the compounds **1a** and **2** and the pyridyl moieties were also probed by infrared spectroscopy. Since both halogen and hydrogen bonding are weaker than covalent and ionic

bonds, it is reasonable to discuss vibrational spectra of the complexes in terms of modified modes of the starting azobenzenes and pyridyl moieties. Pure compounds **3a** and **3b** show a symmetric ring stretching mode at 990 cm<sup>−1</sup>, which exhibits a clear blue-shift of 9 cm<sup>−1</sup> and 21 cm<sup>−1</sup> once complexed with **1a** and **2**, respectively. Similar shifts have been attributed to a reduced electron density over the N atom of the pyridine ring when it is involved as a bond acceptor in the formation of hydrogen and halogen bonding.<sup>[52–54]</sup> The larger the shift, the stronger the interaction the pyridyl is involved in. The blueshifts observed in the IR spectra of the complexes **4–6** suggest that the hydrogen bond given by the azobenzene **2** is stronger than the halogen bond of **1a** (see Supporting Information, Figure S3), thus confirming the energy trend calculated for the 4-methylpyridine dimers of the azobenzenes **1a–c** and **2**.

oxygen bond of **1a** (see Supporting Information, Figure S3), thus confirming the energy trend calculated for the 4-methylpyridine dimers of the azobenzenes **1a–c** and **2**.

#### 2.4. Thin Film Characterization and Photoinduced Surface Patterning

In order to study the SRG formation in halogen-bonded and hydrogen-bonded complexes, we prepared dimethyl formamide (DMF) solutions of the polymer–dye mixtures and spin-cast them as thin films on silicon or glass substrates. In order to prevent dye aggregation and phase segregation, we used relatively low dye/polymer ratios of 0.1 (Figure 3) or 0.2 (Figure 4). The thin films are denoted as P4VP(*i*)<sub>*x*</sub>, where *i* corresponds to the dye molecule in question and *x* is the dye/pyridyl molar ratio. The thin films exhibited similar absorption spectra as measured for the dyes in dilute solutions (see Supporting Information, Figure S2), showing that no excessive dye aggregation takes place in the films.<sup>[55]</sup>

The formation of supramolecular complexes in spin-cast thin films was verified by X-ray photoelectron spectroscopy (XPS), which is a powerful tool for investigating halogen-bonded and hydrogen-bonded complexes in thin films.<sup>[20,56,57]</sup> The binding energies for the I3d doublet of the dye **1a** were

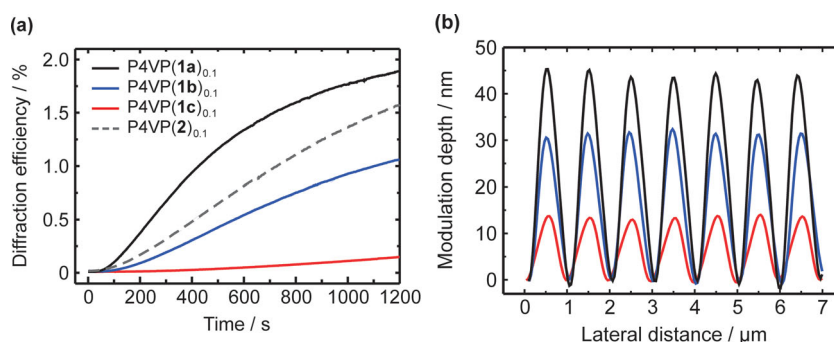


**Figure 3.** Comparison between a) the first-order diffraction efficiency evolution over time and b) the surface profiles of thin films of P4VP(**1a**)<sub>0.1</sub>, P4VP(**1b**)<sub>0.1</sub>, P4VP(**1c**)<sub>0.1</sub>, and P4VP(**2**)<sub>0.1</sub>. The sample thicknesses were 90 nm ± 5 nm. Both the diffraction efficiency and the modulation depth are seen to increase in the order **1c** < **1b** < **2** < **1a**.

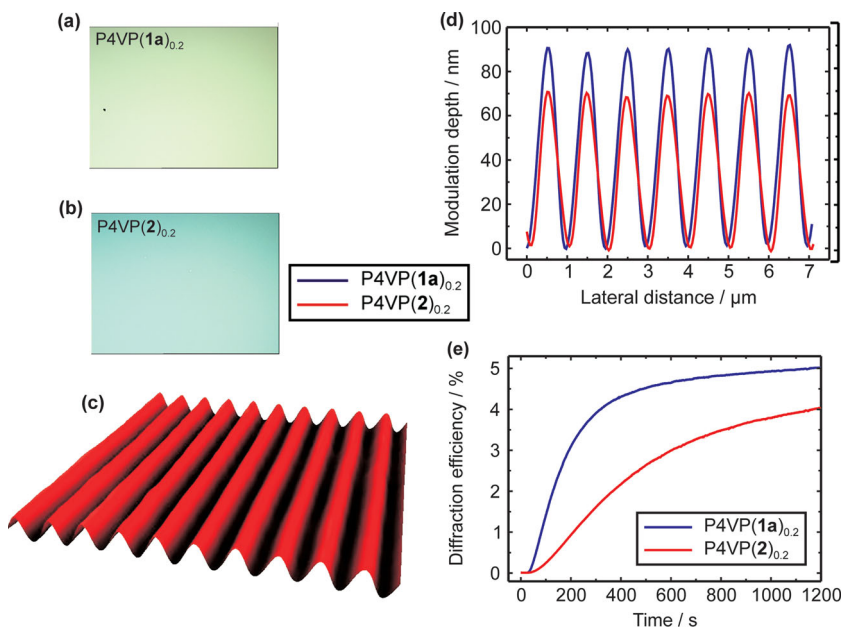


**Figure 4.** Characterization of spin-cast thin films of P4VP(**1a**)<sub>0.2</sub> and P4VP(**2**)<sub>0.2</sub> complexes. The sample thicknesses were ca. 110 nm and 100 nm for the films containing **1a** and **2**, respectively. a, b) Optical microscopy images of thin films of P4VP(**1a**)<sub>0.2</sub> and P4VP(**2**)<sub>0.2</sub>, respectively. c) Atomic force microscopy (AFM) surface profile of the SRG obtained from P4VP(**1a**)<sub>0.2</sub>. d) The surface-modulation depths and e) the time evolution of the first-order diffraction efficiency of a He–Ne probe beam upon the SRG formation.

620.95 eV/632.40 eV in its pure form, and 620.62 eV/632.08 eV in the complex P4VP(**1a**)<sub>0.2</sub>, i.e., they shifted by 0.33 and 0.32 eV to lower energy (Supporting Information, Figure S4a). Similarly, the binding energy of the O1s electron of the dye in the complex P4VP(**2**)<sub>0.2</sub> shifted by 0.66 eV to lower energy upon hydrogen bond formation, from 532.32 eV to 531.66 eV (Supporting Information, Figure S4b). These energy shifts are in excellent agreement with literature values for similar interactions,<sup>[20,56,57]</sup> and they prove that the spin-cast thin films contain halogen- or hydrogen-bonded species. A similar conclusion can also be derived from the analysis of the Fourier transform infrared (FTIR) spectra of the films P4VP(**1a**)<sub>0.2</sub> and P4VP(**2**)<sub>0.2</sub>, which showed several band shifts to lower wave numbers compared to the spectra of the pure dyes (Supporting Information, Table S2).

In order to establish a connection between the SRG inscription efficiency and the nature and strength of the polymer–dye interaction, we compared the grating formation in P4VP(**1a**)<sub>0.1</sub>, P4VP(**1b**)<sub>0.1</sub>, P4VP(**1c**)<sub>0.1</sub>, and P4VP(**2**)<sub>0.1</sub>. First, we estimated the rate of thermal *cis*–*trans* isomerization for the complexes following literature procedures,<sup>[58,59]</sup> and obtained values of  $(11.8 \pm 0.2) \times 10^{-3} \text{ s}^{-1}$ ,  $(13.4 \pm 0.1) \times 10^{-3} \text{ s}^{-1}$ ,  $(12.2 \pm 0.2) \times 10^{-3} \text{ s}^{-1}$ , and  $(13.3 \pm 0.1) \times 10^{-3} \text{ s}^{-1}$  for P4VP(**1a**)<sub>0.1</sub>, P4VP(**1b**)<sub>0.1</sub>, P4VP(**1c**)<sub>0.1</sub>, and P4VP(**2**)<sub>0.1</sub>, respectively. The fact that there is no significant difference in the *cis*-isomer lifetime between the different dyes is important for meaningful comparison of their SRG formation efficiencies.

The films afforded high-quality SRGs upon irradiation with an interference pattern produced with circularly polarized (or *p*-polarized) light. The diffraction efficiencies and grating modulation depths for the  $x = 0.1$  complexes are shown in

Figure 3. The complex with **1c** is the only exception, as it yields essentially no diffraction and only very weak surface modulation, whereas in the halogen-bonded complexes of P4VP with **1a** and **1b** the first-order diffraction efficiency in reflection mode is approximately 3.8% and 2.1% after 20 min of irradiation, respectively. The diffraction efficiencies correlate excellently with the surface profiles (Figure 3b), which show that the modulation depths are ca. 55 nm, 30 nm, and 10 nm for the **1a**, **1b**, and **1c**-based complexes, respectively. The dashed line in Figure 3a corresponds to the diffraction curve for the analogous phenol–pyridine complex P4VP(**2**)<sub>0.1</sub>, the SRG inscription rate of which is slower than for the P4VP(**1a**)<sub>0.1</sub> complex. On the other hand, the inscription performance of the dye **2** exceeds that of the bromine-substituted chromophore **1b**.

Next, we further compared the photopatterning in **1a** and **2**-based complexes using 0.2 dye/pyridyl molar ratios. Both samples displayed high optical quality (Figure 4a and 4b), having an average surface roughness of around 1 nm as measured by AFM. The surface profile for a grating inscribed on P4VP(**1a**)<sub>0.2</sub> film is shown in Figure 4c.

As seen from Figure 4d, the modulation depths of the gratings were ca. 90 nm and 70 nm in favor of the halogen-bonded complex. However, the most striking difference between the halogen- and hydrogen-bonded samples lies in the time evolution of first-order diffraction efficiency, which is commonly used to monitor the build-up of the SRG (Figure 4e). In the case of the halogen-bonded film, the initial slope of the curve, i.e., the SRG inscription efficiency, is significantly higher than for the hydrogen-bonded film, even if their overall diffraction efficiencies in reflection mode upon 20 min of irradiation time are comparable, ca. 5% for P4VP(**1a**)<sub>0.2</sub> and 4% for P4VP(**2**)<sub>0.2</sub>. We note here that when the inscription was performed using *s*-polarized light, essentially no gratings were formed. This evidences the fact that under the experimental conditions used (inscription wavelength 488 nm, irradiation intensity  $300 \text{ mW cm}^{-2}$ , irradiation time 20 min), the grating formation is driven by light-induced mass transport, as opposed to thermal effects, ablation, and photodegradation, which start playing a role at higher irradiation intensities but are polarization-independent.<sup>[13,14]</sup>

### 3. Discussion

Based on the results shown above, the grating formation efficiency develops in the order **1c** < **1b** < **2** < **1a**, which allows us to make two important conclusions. First, the comparison between the complexes involving the dyes **1a**, **1b**, and **1c** attests that the grating formation efficiency is related both to the strength (cf. **1a** and **1b**) and to the nature (cf. **1b** and **1c**) of the noncovalent interactions used. Importantly, the single atom mutation does

not influence the photophysical and electronic properties of the three dyes, which are very similar. Hence, these features do not account for the remarkably different optical performances of the complexes shown in Figure 3. The comparison between **1a** and **1b** is unique, representing to the best of our knowledge the first experimental demonstration of the effect of polymer–azobenzene interaction strength on SRG formation efficiency, even if it has been previously established that covalent/noncovalent bond between the polymer and the azo dyes is required in order for the mass transport to take place.<sup>[12,60]</sup> We emphasize that this is made possible by the unique nature of halogen bonding, which allows one to control the interaction strength by halogen atom substitution while leaving the electronic structure and the photophysical properties of the dyes essentially unaltered.<sup>[41]</sup>

On the other hand, the neatly superior performance of **1b** with respect to **1c** cannot be explained on the basis of interaction strength and photoswitching efficiency alone, since our theoretical studies showed that the interaction energies of the two dyes with the pyridyl moieties as well as their dipole moments have comparable values. We therefore suggest that the higher directionality of halogen bonding with respect to hydrogen bonding provides a more rigid dye–polymer junction, resulting in enhanced mass transport and more efficient SRG inscription. This statement is further supported by the comparison between **1a**- and **2**-based complexes (Figure 4), in which **1a** displays a better performance in spite of a lower binding strength to P4VP. Therefore, our results suggest that halogen-bonded complexes can perform at least as well as analogous hydrogen-bonded polymer–azobenzene complexes in the photopatterning efficiency, and potentially even outperform them.

However, we note that a clear-cut comparison is difficult to make in the latter case, because of the different positioning and bulkiness of **1a** and **2**, and because their electronic structures differ significantly (the absorption maxima of **2** and **1a** are at 415 nm and 470 nm, respectively), which can play a role in the SRG formation.<sup>[49]</sup> Moreover, one might invoke a stronger plasticizing effect on the part of the fluorinated ring, which might ease the polymer chain mobility and result in more efficient grating inscription. As far as the latter effect is concerned, the wide span of performances covered by the fluorinated dyes **1a–c** strongly suggests that this is unlikely to be a major factor. The different positioning of **1a** and **2** with respect to the pyridine moieties may indeed affect the inscription performance, but it should be noted that this factor is not expected to account for the better results obtained for **1b** in comparison to **1c**. Similarly, even if the bulkiness and electronic structure differences are likely to play a role in the SRG formation, they cannot be accounted for as the main elements determining the higher SRG inscription efficiency of P4VP(**1a**)<sub>0.2</sub>. In order to verify whether a higher polymer/dye ratio would play in favour of the hydrogen-bonded complex, we challenged the SRG formation efficiency of P4VP(**1a**)<sub>0.2</sub> with that of P4VP(**2**)<sub>0.33</sub> samples, i.e., higher content of hydrogen bonding dye in the polymer. Moreover, we decided to use in this experiment an irradiation wavelength of 458 nm, instead of the 488 nm used in the previous experiments, since this wavelength is equally absorbed by both dyes (see Supporting Information, Figure S5). Even in those conditions, the **1a**-based complex outperforms

the hydrogen-bonded complex. The above-described results prompt us to propose that there is a relationship among the positive charge localization on the dye, the directionality and rigidity of the polymer–dye interaction, and the SRG formation and efficiency in the studied systems. The sharp localization of the positively charged region in **1a** and **1b** asks for a highly directional interaction with the host polymer matrix. In contrast, the positive charge is hemispherically distributed on the hydrogen atoms of **1c** and **2** resulting in a less directional and, more importantly, less rigid interaction between the polymer and the dye. The conclusion is that not only the strength, but even more importantly the directionality of the noncovalent interaction between the polymer and the photoactive chromophore are to be seen as dominating factors in determining the SRG inscription efficiency in the systems under study.

## 4. Conclusions

Our results not only show that halogen bonding can be used to design supramolecular polymer–azobenzene complexes for photoinduced surface patterning, but also point out that i) the higher directionality of halogen bonding as compared to hydrogen bonding promotes the patterning efficiency and ii) the unique property of halogen bonding to allow fine-tuning of the polymer–dye interaction strength via single halogen atom mutation provides us with fundamental tools for understanding the phenomenon of SRG formation not available in other materials. Such implications are remarkably important in this context, as the underlying mechanism of this fascinating and high-potential photomechanical effect is still under debate. To the best of our knowledge, this is one of the very few reports on the successful use of halogen bonding in the self-assembly of polymer-based systems and the first application of this non-covalent interaction in controlling the properties of light-responsive supramolecular polymers.

## 5. Experimental Section

**Materials and Methods:** The starting materials were purchased from Sigma-Aldrich, Acros Organics, and Apollo Scientific. The dye **2** was purchased from TCI Europe. Commercial high-performance liquid chromatography (HPLC)-grade solvents were used without further purification, except for acetonitrile, which was dried over molecular sieves before use.

<sup>1</sup>H and <sup>19</sup>F NMR spectra were recorded at room temperature on a Bruker AV500 spectrometer, using CDCl<sub>3</sub> or acetone-d<sub>6</sub> as solvents. <sup>1</sup>H NMR chemical shifts were referenced to tetramethylsilane (TMS) using the residual proton impurities of the deuterated solvents as standard reference, while <sup>19</sup>F NMR chemical shifts were referenced to an internal CFCl<sub>3</sub> standard.

The molecular structures of dyes **1a–c** and **2** were optimized for vacuum and for DMF solution using DFT by applying the PBE0 functional and the 6-311++G\*\* basis set for all atoms. Absorption spectra were computed by time-dependent DFT. Accurate interaction energies for the molecular dimers composed of the dyes and 4-methylpyridine, corrected for basis set superposition error ( $\Delta E_{\text{BSSE}}$ ), were computed at PBE0/6-311++G\*\* level as the difference between the energy of the dimer and the sum of the energies of the single monomers. Further details about the theoretical calculations can be found in the Supporting Information.

DSC analysis was performed on a Mettler Toledo DSC823e instrument, using aluminium light 20  $\mu\text{L}$  sample pans and Mettler STARe software for calculation. The melting points were also determined on a Reichert instrument by observing the melting process through an optical microscope. Attenuated total reflectance FTIR (ATR-FTIR) spectra were obtained with a Nicolet Nexus FTIR spectrometer. The values were given in wave numbers and were rounded to  $1\text{ cm}^{-1}$  upon automatic assignment. The X-ray crystal structures were determined on a Bruker Smart Apex II diffractometer. Crystallographic data (excluding structure factors) for the structures reported in this paper have been deposited with the Cambridge Crystallographic Data Centre as supplementary publication no. CCDC-829039; 829040; 829041, 829042. These data can be obtained free of charge via [www.ccdc.cam.ac.uk/data\\_request/cif](http://www.ccdc.cam.ac.uk/data_request/cif). Experimental details about the crystalline structures can be found in the Supporting Information.

The surface-relief gratings were inscribed on thin films spin-cast from freshly prepared DMF solutions of the dye–polymer mixtures on Si substrates. The sample thicknesses were measured with a spectroscopic ellipsometer (Sentech Instruments GmbH, SE805) and double-checked using a DEKTAK 6M surface profiler. The UV-vis spectra were collected using Perkin Elmer Lambda 950 spectrophotometer from both thin films (spin-coated on glass substrates) and diluted ( $10^{-6}\text{ M}$ ) DMF solutions. XPS measurements were performed using an ULVAC-PHI Inc. 1700R ESCA spectrometer equipped with MgK  $\alpha$  X-ray source (1253.6 eV) and hemispherical analyzer. The resolution used was 0.05 eV. The reference spectra of the pure dyes were measured from powders mounted on double-sided carbon tape. The spectra of the complexes were measured from thin films spin coated on silicon substrates. All spectra were referenced to the C1s neutral carbon peak at 284.6 eV.<sup>[55]</sup>

The thermal *cis*–*trans* isomerization was studied by exciting the chromophores with a circularly polarized pump beam (457 nm, 50 mW  $\text{cm}^{-2}$ ) and monitoring the transmittance changes after blocking the pump. The probe was a fiber-coupled xenon lamp equipped with proper bandpass filters. The signal was detected with a photodiode and a lock-in amplifier. The isomerization rate constants were estimated using methods proposed in the literature.<sup>[58,59]</sup> The surface-relief gratings were inscribed using a spatially filtered circularly polarized beam from an Ar<sup>+</sup>-laser ( $\lambda = 488\text{ nm}$  unless otherwise stated), with an irradiation intensity of 300 mW  $\text{cm}^{-2}$ . The interference pattern was created using a Lloyd mirror configuration, with half of the beam directly incident on the sample and the other half reflected from a mirror set at 90° with the sample. The angle between the plane of the mirror and the incident beam was set to 14° to yield an interference pattern with a periodicity of 1  $\mu\text{m}$ . The resulting diffraction gratings were monitored by measuring the first-order diffraction of a low power (<300  $\mu\text{W}$ ; 633 nm) He–Ne laser beam in reflection mode. AFM images used for surface profile characterization were taken with a Veeco Dimension 5000 SPM in tapping mode.

**Synthesis of 4-iodo-2,3,5,6-tetrafluoroaniline:**<sup>[61]</sup> Yellow HgO (1.2 g, 5.5 mmol) was added to a solution of 2,3,5,6-tetrafluoroaniline (1.18 g, 7.2 mmol) in ethanol (20 mL). The solution was vigorously stirred for 30 min at room temperature, then iodine (1.82 g, 7.2 mmol) was added. The mixture was stirred overnight and filtered over celite. The solvent was removed under reduced pressure then the residue was dissolved in  $\text{CH}_2\text{Cl}_2$ . The solution was washed several times first with an aqueous solution of  $\text{Na}_2\text{S}_2\text{O}_3$  (saturated solution), then with pure water. After drying on  $\text{Na}_2\text{SO}_4$  (1 g) the solvent was removed under reduced pressure giving the pure product (1.90 g, yield 90%). m.p. 350 K;  $^1\text{H NMR}$  (500 MHz,  $\text{CDCl}_3$ ,  $\delta$ ) = 4.1 ( $-\text{NH}_2$  broad signal);  $^{19}\text{F NMR}$  (470 MHz,  $\text{CDCl}_3$ ,  $\delta$ ) -124.41 (2 F); -159.90 (2 F); FT-IR:  $\nu_{\text{max}} = 3481, 3387, 1625, 1615, 1598, 1480, 1408, 1347, 1327, 1267, 1171, 1146, 1090, 1051, 975, 915, 800, 712$ .

**General Procedure for the Synthesis of 1a–c:**<sup>[62]</sup> The general procedure for the synthesis of the azobenzene derivatives 1a–c involves the diazobenzene coupling of a tetrafluoroaniline with *N,N*-dimethylaniline. Reactions were carried out in oven-dried glassware under a nitrogen atmosphere, using dry solvents. A solution of the proper 2,3,5,6-tetrafluoroaniline (6 mmol) in dry acetonitrile (10 mL) was added dropwise to a solution of nitrosonium tetrafluoroborate (6 mmol) in

acetonitrile (10 mL) at  $-30\text{ }^\circ\text{C}$ . After 1 h of additional stirring at  $-30\text{ }^\circ\text{C}$  the *N,N*-dimethylaniline (24 mmol) was added dropwise. The resulting solution was stirred overnight at room temperature and then water (30 mL) was added. The mixture was extracted three times with  $\text{CH}_2\text{Cl}_2$ . The organic layers were collected and dried over  $\text{Na}_2\text{SO}_4$ . The solvent was removed under reduced pressure. The residue was purified by recrystallization from methanol.

**1a:** Yield 42%; m.p. = 456 K;  $^1\text{H NMR}$  (500 MHz,  $\text{CDCl}_3$ ,  $\delta$ ) = 7.90 (d 2 H,  $J = 9.2\text{ Hz}$ ), 6.77 (d 2 H,  $J = 9.2\text{ Hz}$ ), 3.15 (s 6 H);  $^{19}\text{F NMR}$  (470 MHz,  $\text{CDCl}_3$ ,  $\delta$ ) -122.48 (2 F), -151.12 (2 F); FTIR:  $\nu_{\text{max}} 2910, 2857, 2804, 2740, 2667, 1596, 1523, 1476, 1393, 1359, 1332, 1308, 1278, 1230, 1144, 1051, 976, 940, 887, 818, 806, 728, 664, 619$ .

**1b:** Yield 40%; m.p. = 444 K;  $^1\text{H NMR}$  (500 MHz,  $\text{CDCl}_3$ ,  $\delta$ ) 7.90 (d 2 H,  $J = 9.4\text{ Hz}$ ), 6.74 (d 2 H,  $J = 9.4\text{ Hz}$ ), 3.13 (s 6 H);  $^{19}\text{F NMR}$  (470 MHz,  $\text{CDCl}_3$ ,  $\delta$ ) -135.48 (2 F), -151.77 (2 F); FTIR:  $\nu_{\text{max}} 2918, 2857, 2810, 2667, 1596, 1519, 1484, 1445, 1395, 1360, 1331, 1309, 1282, 1229, 1176, 1142, 1052, 981, 939, 889, 829, 818, 730$ .

**1c:** Yield 25%; m.p. = 421 K;  $^1\text{H NMR}$  (500 MHz,  $\text{CDCl}_3$ ,  $\delta$ ) 7.90 (d 2 H,  $J = 8.4\text{ Hz}$ ), 6.74 (d 2 H,  $J = 8.4\text{ Hz}$ ), 6.99 (m 1 H), 3.13 (s 6 H);  $^{19}\text{F NMR}$  (470 MHz,  $\text{CDCl}_3$ ,  $\delta$ ) -140.92 (2 F), -153.46 (2 F); FT-IR:  $\nu_{\text{max}} 3082, 2913, 2817, 2667, 1596, 1502, 1359, 1333, 1308, 1278, 1230, 1140, 1035, 954, 865, 819, 758, 734, 714, 687, 663, 629$ .

**Co-crystallization Experiments:** In a typical co-crystallization procedure, the azobenzene derivative and the bis-pyridine compound were separately dissolved in  $\text{CHCl}_3$  or acetone, at room temperature in a 2:1 ratio, under saturated conditions. The two saturated solutions containing the donor and the acceptor were then mixed in a clear borosilicate glass vial, which was left open in a closed cylindrical wide-mouth bottle containing paraffin oil. Solvents were allowed to slowly evaporate at room temperature for a few days until the formation of crystals.

**Co-crystal 4:** m.p. = 465 K; FTIR:  $\nu_{\text{max}} 3076, 3057, 3034, 2994, 2915, 2862, 2806, 2741, 2698, 2667, 1597, 1556, 1524, 1471, 1396, 1362, 1333, 1309, 1276, 1229, 1143, 1071, 1052, 1044, 999, 975, 940, 887, 819, 763, 726$ .

**Co-crystal 5:** m.p. = 446 K; FTIR:  $\nu_{\text{max}} 3070, 2991, 2941, 2900, 2801, 2678, 1586, 1516, 1470, 1423, 1363, 1275, 1254, 1229, 1219, 1195, 1144, 1095, 1070, 1011, 943, 837, 817, 793, 730$ .

**Co-crystal 6:** m.p. = 445 K;  $^1\text{H NMR}$  (500 MHz,  $\text{CDCl}_3$ ,  $\delta$ ) 8.56 (dd 4 H), 7.90 (dd 4 H), 7.23 (dd 4H), 6.75 (dd, 4H), 3.15 (s 12 H), 2.73 (t 4 H), 2.08 (m, 2H);  $^{19}\text{F NMR}$  (470 MHz,  $\text{CDCl}_3$ ,  $\delta$ ) -122.50 (4 F), -151.13 (4 F); FTIR:  $\nu_{\text{max}} 3072, 3034, 2995, 2916, 2859, 2806, 2744, 2666, 1597, 1557, 1521, 1472, 1444, 1419, 1394, 1362, 1335, 1309, 1273, 1231, 1146, 1067, 1041, 1000, 972, 943, 887, 818, 805, 798$ .

**Mechanochemical Synthesis of the Azobenzene Complexes:** Solid-state reactions were carried out using a Retsch MM400 ball mill with 5.0 mL vessels. 1,3-di(4-pyridyl)propane (**3b**) was mixed with 2 equivalents of azobenzenes 1a–c and **2** in a 5 mL grinding jar. The reactants were ground at 30 Hz for 60 min. This procedure resulted in the quantitative formation of the co-crystals **5** and **6**, starting from **1a** and **2**, while grinding **3b** with **1b** or **1c** gave just a mechanical mixture of the two starting compounds.

## Supporting Information

Supporting Information is available from the Wiley Online Library or from the author.

## Acknowledgements

A.P. acknowledges the financial support provided by the Japanese Society for the Promotion of Science and the Foundations' Post Doc Pool in Finland. This work was also partially funded by the Academy of Finland (PHORMAT project; 135106). P.M. and G.R. acknowledge the Cariplo Foundation (projects 2150 and 2010-1351) for financial support. A.F. acknowledges the CINECA Award N. \*\*HP10BFJG1H 2011

'IscrB\_HEChro', for the availability of high performance computing resources and support. Prof. Baba and Prof. Motokura from Tokyo Tech are greatly acknowledged for their kind assistance with XPS spectroscopy.

Received: January 15, 2012

Revised: February 14, 2012

Published online:

- [1] P. Rochon, E. Batalla, A. Natansohn, *Appl. Phys. Lett.* **1995**, *66*, 136.
- [2] N. K. Viswanathan, D. Y. Kim, S. Bian, J. Williams, W. Liu, L. Li, L. Samuelson, J. Kumar, S. K. Tripathy, *J. Mater. Chem.* **1999**, *9*, 1941.
- [3] Y. Morikawa, S. Nagano, K. Watanabe, K. Kamata, T. Iyoda, T. Seki, *Adv. Mater.* **2006**, *18*, 883.
- [4] C. Hubert, A. Rumyantseva, G. Lerondel, J. Grand, S. Kostcheev, L. Billot, A. Vial, R. Bachelot, P. Royer, *Nano Lett.* **2005**, *5*, 615.
- [5] S. Lee, H. S. Kang, J.-K. Park, *Adv. Funct. Mater.* **2011**, *21*, 1770.
- [6] A. Kravchenko, A. Shevchenko, V. Ovchinnikov, A. Priimagi, M. Kaivola, *Adv. Mater.* **2011**, *23*, 4174.
- [7] T. Ubukata, T. Seki, K. Ichimura, *Adv. Mater.* **2000**, *12*, 1675.
- [8] B. Darracq, F. Chaput, K. Lahlil, Y. Levy, J. P. Boilot, *Adv. Mater.* **1998**, *10*, 1133.
- [9] H. Nakano, T. Tanino, T. Takahashi, H. Ando, Y. Shirota, *J. Mater. Chem.* **2008**, *18*, 242.
- [10] J. Gao, Y. He, F. Liu, X. Zhang, Z. Wang, X. Wang, *Chem. Mater.* **2007**, *19*, 3877.
- [11] O. Kulikovska, L. M. Goldenberg, J. Stumpe, *Chem. Mater.* **2007**, *19*, 3343.
- [12] N. Zettsu, T. Ogasawara, N. Mizoshita, S. Nagano, T. Seki, *Adv. Mater.* **2008**, *20*, 516.
- [13] O. N. Oliveira, J. Kumar, L. Li, S. K. Tripathy, in *Photoreactive Organic Thin Films* (Eds: Z. Sekkat, W. Knoll) Academic Press, San Diego, CA **2002**, Ch. 14.
- [14] K. G. Yager, C. J. Barrett, in *Smart Light-Responsive Materials*, (Eds: Y. Zhao, T. Ikeda), John Wiley & Sons Inc., Hoboken, NJ **2009**, Ch. 4.
- [15] O. Hassel, Nobel Lecture, 9 June 1970.
- [16] An IUPAC Task Group set up to examine the definition of halogen bonding has not yet reported, so that given here should be taken as temporary. See the IUPAC website [www.iupac.org/web/ins/2009-032-1-100](http://www.iupac.org/web/ins/2009-032-1-100) and the website of the project on halogen bonding: [www.halogenbonding.eu](http://www.halogenbonding.eu), (accessed March 2012).
- [17] P. Metrangolo, H. Neukirch, T. Pilati, G. Resnati, *Acc. Chem. Res.* **2005**, *38*, 386.
- [18] H. Loc Nguyen, P. N. Horton, M. B. Hursthouse, A. C. Legon, D. W. Bruce, *J. Am. Chem. Soc.* **2004**, *126*, 16.
- [19] J. Xu, X. Liu, C. He, *Macromolecules* **2005**, *38*, 3554.
- [20] J. Xu, X. Liu, J. K.-P. Ng, T. Lin, C. He, *J. Mater. Chem.* **2006**, *16*, 3540.
- [21] D. W. Bruce, P. Metrangolo, F. Meyer, T. Pilati, C. Präsang, G. Resnati, G. Terraneo, S. Wainwright, A. C. Whitwood, *Chem. Eur. J.* **2010**, *16*, 9511.
- [22] P. Metrangolo, Y. Carcenac, M. Lahtinen, T. Pilati, K. Rissanen, A. Vij, G. Resnati, *Science* **2009**, *323*, 1461.
- [23] A. Abate, M. Brischetto, G. Cavallo, M. Lahtinen, P. Metrangolo, T. Pilati, S. Radice, G. Resnati, K. Rissanen, G. Terraneo, *Chem. Commun.* **2010**, *46*, 2724.
- [24] M. Fourmigue, P. Batail, *Chem. Rev.* **2004**, *104*, 5379.
- [25] O. Bolton, K. Lee, H. J. Kim, K. Y. Lin, J. Kim, *Nat. Chem.* **2011**, *3*, 205.
- [26] A. Mele, P. Metrangolo, H. Neukirch, T. Pilati, G. Resnati, *J. Am. Chem. Soc.* **2005**, *127*, 14972.
- [27] A. R. Voth, P. Khoo, K. Oishi, P. S. Ho, *Nat. Chem.* **2009**, *1*, 74.
- [28] A. Farina, S. V. Meille, M. T. Messina, P. Metrangolo, G. Resnati, G. Vecchio, *Angew. Chem. Int. Ed.* **1999**, *38*, 2433.
- [29] a) P. Metrangolo, F. Meyer, T. Pilati, G. Resnati, G. Terraneo, *Angew. Chem. Int. Ed.* **2008**, *47*, 6114; b) K. Rissanen, *CrystEngComm* **2008**, *9*, 1107.
- [30] R. Bertani, P. Metrangolo, A. Moiana, E. Perez, T. Pilati, G. Resnati, I. Rico-Lattes, A. Sassi, *Adv. Mater.* **2002**, *14*, 1197.
- [31] T. Takeuchi, Y. Minato, M. Takase, H. Shinmori, *Tetrahedron Lett.* **2005**, *46*, 9025.
- [32] a) N. S. Goroff, S. M. Curtis, J. A. Webb, F. W. Fowler, J. W. Lauher, *Org. Lett.* **2005**, *7*, 1891; b) A. Sun, J. W. Lauher, N. S. Goroff, *Science* **2006**, *312*, 1030.
- [33] T. Shirman, D. Freeman, Y. D. Posner, I. Feldman, A. Facchetti, M. E. van der Boom, *J. Am. Chem. Soc.* **2008**, *130*, 8162.
- [34] L. Brunsveld, B. J. B. Folmer, E. W. Meijer, R. P. Sijbesma, *Chem. Rev.* **2001**, *101*, 4071.
- [35] M. Weck, *Polym. Int.* **2007**, *56*, 453.
- [36] T. Kato, N. Mizoshita, K. Kishimoto, *Angew. Chem. Int. Ed.* **2006**, *45*, 38.
- [37] M. R. Hammond, R. Mezzenga, *Soft Matter* **2008**, *4*, 952.
- [38] G. ten Brinke, O. Ikkala, *Chem. Rec.* **2004**, *4*, 219.
- [39] P. Politzer, J. S. Murray, T. Clark, *Phys. Chem. Chem. Phys.* **2010**, *12*, 7748.
- [40] P. Metrangolo, F. Meyer, T. Pilati, G. Resnati, G. Terraneo, *Chem. Commun.* **2008**, 1635.
- [41] P. Politzer, P. Lane, M. C. Concha, Y. Ma, J. S. Murray, *J. Mol. Model.* **2007**, *13*, 305.
- [42] A. Priimagi, K. Lindfors, M. Kaivola, P. Rochon, *ACS Appl. Mater. Interfaces* **2009**, *1*, 1183.
- [43] J. Vapaavuori, A. Priimagi, M. Kaivola, *J. Mater. Chem.* **2010**, *20*, 5260.
- [44] T. Alasaarela, D. Zheng, L. Huang, A. Priimagi, B. Bai, A. Tervonen, S. Honkanen, M. Kuittinen, J. Turunen, *Opt. Lett.* **2011**, *36*, 2411.
- [45] J. Vapaavuori, V. Valtavirta, T. Alasaarela, J. Mamiya, A. Priimagi, A. Shishido, M. Kaivola, *J. Mater. Chem.* **2011**, *21*, 15437.
- [46] A. Forni, *J. Phys. Chem. A* **2009**, *113*, 3403.
- [47] M. D. Joeston, R. S. Drago, *J. Am. Chem. Soc.* **1962**, *84*, 3817.
- [48] E. Corradi, S. V. Meille, M. T. Messina, P. Metrangolo, G. Resnati, *Angew. Chem. Int. Ed.* **2000**, *39*, 1782.
- [49] C. J. Barrett, A. L. Natansohn, P. L. Rochon, *J. Phys. Chem.* **1996**, *100*, 8836.
- [50] A. Bondi, *J. Phys. Chem.* **1964**, *68*, 441.
- [51] P. Metrangolo, G. Resnati, T. Pilati, S. Biella, in *Halogen Bonding Fundamentals and Applications*, (Eds: P. Metrangolo, G. Resnati), Springer, Berlin, Germany **2008**, Ch. 4, pp. 105–136.
- [52] L. C. Cesteros, J. R. Isasi, I. Katime, *Macromolecules* **1993**, *26*, 7256.
- [53] J. Ruokolainen, G. ten Brinke, O. Ikkala, M. Torkkeli, R. Serimaa, *Macromolecules* **1996**, *29*, 3409.
- [54] A. Priimagi, J. Vapaavuori, F. J. Rodriguez, C. F. J. Faul, M. T. Heino, O. Ikkala, M. Kauranen, M. Kaivola, *Chem. Mater.* **2008**, *20*, 6358.
- [55] A. Priimagi, S. Cattaneo, R. H. A. Ras, S. Valkama, O. Ikkala, M. Kauranen, *Chem. Mater.* **2005**, *17*, 5798.
- [56] X. Zhou, S. H. Goh, S. Y. Lee, K. L. Tan, *Appl. Surf. Sci.* **1997**, *119*, 60.
- [57] F. Wang, N. Ma, Q. Chen, W. Wang, L. Wang, *Langmuir* **2007**, *23*, 9540.
- [58] C. S. Paik, H. Morawetz, *Macromolecules* **1972**, *5*, 171.
- [59] C. Barrett, A. Natansohn, P. Rochon, *Chem. Mater.* **1995**, *7*, 899.
- [60] C. Fiorini, N. Prudhomme, G. de Veyrac, I. Maurin, P. Raimond, J.-M. Nunzi, *Synth. Met.* **2000**, *115*, 121.
- [61] H. H. Wenk, W. Sander, *Angew. Chem. Int. Ed.* **2002**, *41*, 2742.
- [62] R. Weiss, F. G. Puhlhofer, *J. Am. Chem. Soc.* **2007**, *129*, 547.